SELF-PROPAGATING COMBUSTION SYNTHESIS VIA AN MSR PROCESS: AN EFFICIENT AND SIMPLE METHOD TO PREPARE (Ti, Zr, Hf)B_2-Al_2O_3 POWDER NANOCOMPOSITES

M. J. Sayagués*, M. A. Avilés, J.M. Córdoba and F. J. Gotor

Instituto de Ciencia de Materiales de Sevilla (CSIC-US), Américo Vespucio 49, 41092 Sevilla, SPAIN.

* Corresponding author: *sayagues@cica.es*

Abstract

The synthesis of **$(Ti_{1-x}Zr_x)B_2$-Al_2O_3**, **$(Ti_{1-x}Hf_x)B_2$-Al_2O_3** and **$(Zr_{1-x}Hf_x)B_2$-Al_2O_3** (x=0, 0.5 and 1) powder nanocomposites via a mechanochemical method using TiO_2, ZrO_2, HfO_2, HBO_2 and Al as the raw materials was investigated. The formation of the nanocomposites proceeds via a mechanically-induced self-sustaining reaction (MSR) process that involves several simultaneous reactions. The aluminothermic reductions of the T_MO_2 and HBO_2 produce Al_2O_3 and transition metal and boron elements, which in turn react to yield the diboride phase. The ignition of the complex combustion reaction occurred after a short milling time (15-30 min), instantly transforming most of the reactants into products. The sample composition was marked by the stoichiometry of the combustion reaction, and the resulting nanocomposites were analysed using XRD, ED, SEM, TEM and EDX techniques. The X-ray results confirmed the biphasic character of the prepared composite powder (T_MB_2 and Al_2O_3 structures); minor amounts of the Zr and Hf oxides were also observed. The achieved microstructure was characterised by the agglomeration of Al_2O_3 nanocrystallites and diborides crystals with a diffraction domain size ranging between 100 and 300 nm.

1. INTRODUCTION

Ti, Zr and Hf diborides are significant materials because their properties make them suitable for high performance applications, such as impact resistant armours, cutting tools, wear resistant coatings, molten metal crucibles and high temperature electrodes. These materials offer high melting points, hardness and elastic modulus values, good thermal and electrical conductivities, low thermal expansion coefficients, chemical inertness, high thermal stabilities, and excellent wear and oxidation resistances [1]. The three diborides possess the same AlB_2-type structure and can form solid solutions [2, 3], which has been proposed as an approach to improve the properties of the final material [4]. However, the use of these materials is currently limited due to their low level of sinterability.

These metal diborides have been mixed with other refractory ceramics such as Al_2O_3 to produce more dense materials without damaging the properties. Two different methods have been used to prepare these composites. The first and most effective method is to prepare the composite *in-situ* starting from the metal oxide, boron oxide or boric acid and Al or Mg [5-20], which generally proceeds through a complex self-propagating or combustion reaction. The second method is to obtain the two phases separately and to then produce a mixture of both phases [21-23]. A large number of investigations have been performed in both cases, although we will highlight select studies that have been performed using combustion reactions. Mishra et al. [5-8] synthesised ZrB_2-Al_2O_3 nanocomposites using a self-propagating high-temperature synthesis process (SHS), an advanced method that has been used extensively for preparing refractory materials. Mousavian et al. used a mechanical activation process to aid microwave-assisted combustion synthesis to produce a TiB_2–Al_2O_3 composite [9] and studied the effect of mechanical activation on the SHS synthesis to obtain the same composite [10].

Self-sustaining reactions can be initiated not only using heat, as in an SHS process, but also by mechanical energy during the milling of highly exothermic mixtures. This type of mechanochemical process is called a mechanically induced self-sustaining reaction (MSR) [24], and the critical milling time required to ignite the mixture is called the ignition time (t_{ig}). Sharifi et al. [11] proposed a mechanochemical processing to prepare a TiB_2–Al_2O_3 nanocomposite and reported that during the ball milling in a planetary mill, the $Al/B_2O_3/Ti$ mixture reacted in a combustion mode after 30 hours at 500 rpm. The same nanocomposite powder was prepared by Rabiezadeh et al. [12, 13] by combining sol-gel and mechanochemical methods. In their study, the nanocomposite was obtained after milling a mixture of a dried gel (containing B and Ti) and Al powder for 30 hours at 300 rpm, without any evidence of the occurrence of an MSR process. Magnesium was used as an alternative to aluminium by Welham [14-16] and Akgun et al. [17] to synthesise TiB_2 and ZrB_2 from $TiO_2/B_2O_3/Mg$ or $ZrO_2/B_2O_3/Mg$, respectively, using a ball-milling technique. Long milling times were always required, and no combustion reactions were reported.

In this work, the synthesis of **$(Ti_{1-x}Zr_x)B_2$-Al_2O_3**, **$(Ti_{1-x}Hf_x)B_2$-Al_2O_3** and **$(Zr_{1-x}Hf_x)B_2$-Al_2O_3** (x=0, 0.5 and 1) composite materials, in which the diboride phase is formed by a solid solution of two transition metals, was investigated. The process was conducted using the MSR mechanochemical method starting from stoichiometric mixtures of TiO_2, ZrO_2, HfO_2, HBO_2 and Al. This study demonstrates that the composite materials can be formed by high-energy ball milling, inducing a self-sustaining reaction without an external heat supply and in a short time.

2. EXPERIMENTAL PROCEDURE

Titanium oxide (anatase TiO_2; 99%, Aldrich), zirconium oxide (ZrO_2; 99%, Aldrich), hafnium oxide (HfO_2; 99%, Alfa Aesar), metaboric acid (HBO_2; 98%, Fluka, dried at 110ºC) and aluminium (Al; 99%, Aldrich) powders were used in this work. The appropriate powder mixtures according to the stoichiometric quantities fixed by equations (1) to (6) (table I) were ball-milled under 6 bars of high-purity argon gas (Linde) to avoid oxidation using a modified planetary ball-mill (Pulverisette 7, Fritsch). Then, 5 g of the powder reactive mixture and seven tempered steel balls were placed in a tempered steel vial (67 HRC) for each milling experiment. The volume of the vial was 45 mL. The diameter and weight of balls were 15 mm and 12.39 g, respectively, and the powder-to-ball mass ratio (PBR) was 1/17.5. A spinning rate of 600 rpm was used. The vial was purged with argon gas several times, and the desired pressure was selected before milling. The vial was connected to the gas cylinder during the grinding experiments by a rotary valve and a flexible polyamide tube. The argon pressure was continuously monitored during the milling process with an SMC solenoid valve (model EVT307-5DO-01F-Q, SMC Co.) and recorded in a paperless device (RSG30 Ecograph T, Endress+Hauser). When a self-sustaining reaction occurs, the increasing temperature due to the exothermic reaction produces an instantaneous increase in the total pressure. The ignition time ($\mathbf{t_{ig}}$) was thus determined from the time–pressure record.

X-ray diffraction (XRD) analysis was performed on a PANalytical X´Pert PRO diffractometer equipped with a graphite diffracted beam monochromator and a solid state detector (X´Cellerator) with an angular aperture of 2.12º (2Θ) using Cu Kα radiation (45 KV, 40 mA). The data were collected over a 2Θ-range of 20º to 150º using a step size of 0.017º and a counting time of 300 s/step. The Rietveld refinement method using the freely distributed programme FULLPROF was employed for refinement of the cell parameters in the diboride solid solutions and for the quantitative phase analysis of composite products.

Scanning electron microscopy (SEM) was performed using a Hitachi FEG S-4800 microscope. Transmission electron microscopy (TEM), electron diffraction (ED) and energy dispersive X-ray spectroscopy (EDX) were performed in a Philips CM-200 microscope operating at 200 kV with a LaB_6 filament (point resolution of 2.3 Å) and EDAX analysis system.

3. RESULTS AND DISCUSSION

All the reactants were analysed using X-ray diffraction and SEM techniques; the results are presented in Figure 1, and the structural parameters are listed in table II. The Al powder is highly crystalline and shaped by large micrometric round particles, which are formed by smaller crystallites. The HBO_2 is also a crystalline material with a smaller particle size. These two reactants were used for all the MSR reactions, and the transition metal ($\mathbf{T_M}$) oxides were varied as indicated in equations (1) to (6). The three transition metal oxides were formed by small round particles with similar mean particle sizes and shapes, which benefit the viability of obtaining similar results for all the composite materials.

The preparation of 6 different nanocomposites formed by diboride and Al_2O_3 phases in a molar ratio of 3/5 was attempted; the nomenclature of these nanocomposites is presented in table I. In a first attempt, stoichiometric amounts of the starting materials were mixed to obtain the **T** composite (equation 1) and milled under the aforementioned conditions. An abrupt increase in the pressure was observed in the time-pressure record after 16.5 min of milling (Fig. 2), which is a clear indication that a combustion or self-sustaining reaction occurred. The large increase in the pressure is due to the increase in temperature; the ball collisions with powder reactants activate the mixture until the reaction starts, and a large

amount of heat is liberated, producing a self-propagating front that spread out instantaneously. Then, the pressure suddenly decreases and reaches the starting value in a few seconds.

For the **T** composite, milling was stopped directly after ignition (16.5 min), and the obtained powder ($\mathbf{T_a}$) was analysed by XRD (Fig. 3). The XRD pattern reveals the formation of the diboride and Al_2O_3 phases in addition to a minor amount of reagents. Using the ball-milling technique, we have obtained a composite powder in a very short time compared with the literature data for similar methods [11-15]. When the same experiment was repeated with the milling process continued for two hours to complete the reaction after combustion, the XRD pattern (Fig. 3) indicates that the reactants disappeared and a full conversion was attained. Peak broadening is observed due to the extended milling process, which decreased the coherent diffraction domains. The other five reactions were performed under the same conditions (2 hours of total milling), and the time-pressure records (Fig. 2) indicated that ignition was possible for all of the reactions. The successful synthesis of the intended composite materials was confirmed by XRD measurements (Fig. 4).

All the combustion reactions occurred after a short milling time (16-24 minutes), as observed in table I and Figure 3. It is not easy to evaluate the slight differences in time observed as the global reactions (1) to (6) are composed of several semi-reactions that simultaneously occur. The formation of each T_MB_2-Al_2O_3 nanocomposite implies three or four semi-reactions (table I); the first two or three are aluminothermic reactions, yielding Al_2O_3, B and T_M. The reduction of HBO_2 by Al most likely initiates the process as it is a very exothermic self-propagating reaction (ΔH°=-1132.50 kJ) and is common for all the systems. Concerning the transition metal oxides, TiO_2 reduction is the more exothermic reaction (ΔH°=-527.20 kJ) compared with the ZrO_2 (ΔH°=-49 kJ) and HfO_2 (ΔH°=1.1 kJ) reductions and can proceed through an MSR process. However, the reductions of ZrO_2 and HfO_2 by Al are not viable as self-propagating reactions even though the reactions were triggered by the

liberated heat from the HBO_2 aluminothermy. The last concerned reaction is the synthesis of the binary or ternary diboride phases from the mixture of their elements obtained in the previous aluminothermic reactions. These mechanochemical reactions of the formation of binary and ternary (solid solution) diborides have been already reported [2, 3] and can also proceed via an MSR process, which is consistent with their high exothermic character (table I).

However, it could be experimentally appreciated (Fig. 2) that the pressure inside the jar increases as more heat is released in the processes; in this manner, the attained pressure for reactions (1), (2) and (3), in which three different semi-reactions are involved, increases from (1) to (3). A similar tendency was observed for reactions (4), (5) and (6), in which four different semi-reactions occur. Nevertheless, a constant weight of reactants (5 g) was set for all the reactions, which means that the number of moles involved in each process was not constant.

As stated previously, the XRD analysis revealed that the six composites are formed by a hexagonal diboride phase (*P6/mmm*) and a rhombohedral Al_2O_3 phase (corundum *R-3c*). Only small amounts of ZrO_2 and HfO_2 were detected in the **Z**, **H**, **TZ, TH** and **ZH** samples. To confirm the formation of solid solution diboride phases, the obtained **T-TZ-Z** (Fig. 4a), **T-TH-H** (Fig. 4b) and **Z-ZH-H** (Fig. 4c) diffractograms corresponding to the same system were compared. The three solid solutions were formed, as can be appreciated by observing that the 2Θ position of the reflexions of the ternary diboride phases appeared just in between those of the two binary diboride phases. Although the Al_2O_3/T_MB_2 molar ratio was 5/3 (table I) for all the samples, the relative intensity of the Al_2O_3 XRD peaks decreased from Ti < Zr < Hf because of the lower X-ray scattering factor as the atomic number decreased. To verify the phase proportion in each sample, Rietveld analysis was performed, and the fitting results as well as the lattice parameters for the binary and ternary diboride phases are presented in table

III. The calculated proportion in weight of the phases is consistent with the expected stoichiometry (table I) considering the amount of unreacted metal transition oxide. The lattice parameters of the ternary diborides exhibit the typical shift characteristic of a solid solution because of the partial substitutions of Ti, Zr and/or Hf in the (0,0,0) position of the AlB_2-type structure.

Microstructural characterisation of the six powder nanocomposites was performed using scanning and transmission electron microscopy techniques (SEM, EDX-mapping TEM, ED and EDX), and representative results are presented in figs 5 and 6. The SEM micrographs (Fig. 5a) show the morphology and particle size distribution of the six samples. All the materials are quite similar and are formed by agglomerates, in which faceted (100-200 nm) and rounded particles can be distinguished. In the **T-Z-H** series, the particle size decreases from **T** to **H,** and consequently, the same trend was observed in the **TZ-TH-ZH** series. Due to the great agglomeration of particles, it is almost impossible to distinguish the Al_2O_3 and diboride phases in the image contrast. EDX-mapping experiments were performed to analyse the element distribution, and the results for the **TH** composite are presented in Figure 5b, where the secondary electron image and the Al, Ti and Hf elemental maps are shown. From the coloured maps, it can be assumed that the large particle in the middle of the image corresponds to Al_2O_3 and that the diboride phase is a solid solution, which is supported by the similarity of the Ti and Hf maps. A good distribution of the constituent phases in the composite material can also be inferred.

Two representative TEM micrographs corresponding to the **T** and **TH** powder nanocomposites are presented in Figure 6 and confirm the agglomerated particle distribution observed by SEM. An ED study established that the larger diffraction domains correspond to the diboride phase, TiB_2 in the **T** composite and $(Ti,Hf)B_2$ in the **TH** composite (marked in image Fig. 6), with a hexagonal symmetry and *P6/mmm* space group. The TiB_2 ED pattern

was oriented along the [*101*] zone axis, and the (Ti,Hf)B_2 ED pattern was oriented along the [001] zone axis. The smallest diffraction domains correspond to the Al_2O_3 phase in both nanocomposites, as observed in the ED rings (Fig. 6, **T** and **TH**), where all of the d spacing can be indexed in the corundum rhombohedral symmetry, *R-3c* space group. The ED results are supported by EDX analysis, and the spectra taken in the same regions as the ED patterns show Al and O in the Al_2O_3 region and Ti or Ti and Hf in the diboride area (Fig. 6, **T** and **TH**). These results confirm the formation of a diboride solid solution. After many ED and EDX analyses, it can be concluded that the two phases are homogeneously distributed throughout the powder samples.

4. CONCLUSIONS

Six powder nanocomposites (**TiB_2-Al_2O_3**, **ZrB_2-Al_2O_3**, **HfB_2-Al_2O_3**, **$(Ti_{0.5}Zr_{0.5})B_2$-Al_2O_3**, **$(Ti_{0.5}Hf_{0.5})B_2$-Al_2O_3** and **$(Zr_{0.5}Hf_{0.5})B_2$-Al_2O_3**) were successfully synthesised using a mechanochemical method, starting from a mixture of very simple and inexpensive reactants (Al, HBO_2 and Ti, Zr or Hf oxide powders). Additionally, this method can be completed in a short milling time (approximately 30 minutes), which can reduce contamination problems.

The analysis of the experimental results in this work demonstrated that a mechanically induced self-sustaining reaction (MSR) process occurred during milling. This process can be useful for the synthesis of powder nanocomposite materials, even for complex system involving several reactions. The ability of the MSR process to tailor the chemical composition of composite materials belonging to the Ti-Zr-Hf diboride- Al_2O_3 system was demonstrated.

The microstructural characterisation of the composite powders revealed an excellent distribution of the two phases, nanometric Al_2O_3 particles in all of the powders and Ti, Zr, Hf

binary or ternary diboride phases with micrometric faceted particles. The formation of diboride solid solutions was confirmed using various characterisation techniques.

Acknowledgments

This work was supported by the Spanish government under grant No. MAT2011-22981, which is financed in part by the European Regional Development Fund of 2007–2013. J. M. Córdoba was supported by CSIC through JAE-Doc grant, which is financed in part by the European Social Fund (ESF).

5. REFERENCES

[1] R. Telle, L.S. Sigl, K. Takagi, Boride-based hard materials, in: R. Riedel (Ed.), Handbook of Ceramic Hard Materials, vol. 2, Wiley-VCH, Weinheim (2000) 802–945.

[2] M.A. Avilés, J.M. Córdoba, M.J. Sayagués, M.D. Alcalá, F.J. Gotor, Mechanosynthesis of $Hf_{1-x}Zr_xB_2$ Solid Solution and $Hf_{1-x}ZrxB_2$/SiC Composite Powders, Journal of American Ceramic Society 93 (2010) 696–702.

[3] M.A. Avilés, J.M. Córdoba, M.J. Sayagués, F.J. Gotor, Mechanochemical synthesis of $Ti_{1-x}Zr_xB_2$ and $Ti_{1-x}Hf_xB_2$ solid solutions, Ceramic International 37 (2011) 1895–1904.

[4] V. Chauvel-Kokabi, K. Shobu, T Watanabe. Studies of the mechanical properties of TiB_2–6%TaB_2–1%CoB–x%mZrO_2. Journal of European Ceramic Society 17 (1997) 885–890.

[5] S.K., Mishra, L.C. Pathak, S.K. Das, P. Ramachandrarao, DYu. Belov, S. Mamyan, Synthesis of Zirconium Diboride-Alumina Composite by the Self-Propagating High-Temperature Synthesis Process, Metallurgic & Material Transition 34A (2003) 1979–1983.

[6] S.K. Mishra, P.K.P. Rupa, S.K. Das, V. Shcherbakov, Effect of Alumina Diluent on the Fabrication of In-Situ Al_2O_3–Ti/ZrB_2 Composite by Self Propagating High Temperature Synthesis Dynamic Compaction, Metallurgic & Material Transition. Trans. 37B (2006) 641–647.

[7] S.K. Mishra, S.K. Das, L.C. Pathak, Sintering behaviour of self-propagating high temperature synthesised ZrB_2–Al_2O_3 composite powder, Material Science & Engineering A 106 (2006) 229–234.

[8] S.K. Mishra, S.K. Das, V. Sherbacov, Fabrication of Al_2O_3–ZrB_2 in situ composite by SHS dynamic compaction: A novel approach, Composite Science & Technology 67 (2007) 2447–2453.

[9] R.T. Mousavian, S. Sharafi, M.H. Shariat, Microwave-assisted combustion synthesis in a mechanically activated Al–TiO_2-H_3BO_3 system, International Journal of Refractory Metal and Hard Materials 29 (2011) 281–288.

[10] R.T. Mousavian, S. Sharafi, M.R. Roshan, M.H. Shariat, Effect of mechanical activation of reagents mixture on the high-temperature synthesis of Al_2O_3–TiB_2 composite powder, Journal of Thermal Analysis and Calorimetry 104 (2011) 1063–1070.

[11] E.M. Sharifi, F. Karimzadeh, M.H. Enayati, Preparation of Al_2O_3–TiB_2 nanocomposite powder by mechanochemical reaction between Al, B_2O_3 and Ti, Advanced Powder Technology 22 (2011) 526–531.

[12] A. Rabiezadeh, A.M. Hadian, A. Ataie, Preparation of alumina/titanium diboride nano-composite powder by milling assisted sol–gel method, International Journal of Refractory Metal and Hard Materials 31 (2012) 121–124.

[13] A. Rabiezadeh, A. Ataie, A.M. Hadian, Sintering of Al_2O_3–TiB_2 nano-composite derived from milling assisted sol–gel method, International Journal of Refractory Metal and Hard Materials (2012) 33 58–64.

[14] N.J. Welham, Formation of TiB_2 from rutile by room temperature ball milling, Mineral Engineering 12 1213–1224 (1999).

[15] N.J. Welham, Formation of nanometric TiB_2 from TiO_2, Journal of American Ceramic Society 83 (2000) 290–292.

[16] N. Setoudeh, N.J. Welham, Formation of zirconium diboride (ZrB_2) by room temperature mechanochemical reaction between ZrO_2, B_2O_3 and Mg, Journal of Alloys and Compounds. 420 (2006) 225–28.

[17] B. Akgun, H.E. Camurlu, Y. Topkaya, N. Sevinc. Mechanochemical and volume combustion synthesis of ZrB2, International Journal of Refractory Metal and Hard Materials 29 (2011) 601–607.

[18] J. Li, Z. Cai, H. Guo, B. Xu, L. Li, Characteristics of porous Al_2O_3–TiB_2 ceramics fabricated by the combustion synthesis, Journal of Alloys and Compounds 479 (2009) 803–806 (2009).

[19] W. Wang, Z. Fu, H. Wang, R. Yuan,Chemistry reaction processes during combustion synthesis of B_2O_3–TiO_2–Mg system, Journal of Material Processing and Technology. 128 (2002)162-168.

[20] D. Wang, Effects of additives on combustion synthesis of Al_2O_3–TiB_2 ceramic composite, J. Eur. Ceram. Soc. 29 (2009) 1485–1492.

[21] P. Li, W. Zhou, J. Zhu, F. Luo, D. Zhu, Influence of TiB_2 content and powder size on the dielectric property of TiB_2/Al_2O_3 composites, Scripta Materiala 60 (2009) 760–763.

[22] Z. Jinyong, T. Wenjun, F. Zhengyi, W. Weiming, Z. Qingjie, Fabrication of Homogenous Dispersion TiB_2-Al_2O_3 Composites, Journal of Wuhan University of Technology-Materials (2011) 681–683.

[23] L. Guoxi, Y. Dongming, Z. Jinyong, Microstructure and Mechanical Properties of TiB_2-Al_2O_3 Composites, Journal of Wuhan University of Technology-Materials (2011) 696– 699.

[24] L. Takacs, Self-Sustaining Reactions Induced by Ball Milling, Progress in Material Science 47 (2002) 355–414.

[25] M. Binnewies, E. Milke, Thermochemical Data of Elements and Compounds, edited by Wiley–VCH (Germany 1999).

FIGURE CAPTIONS

Figure 1. X-ray diffraction patterns of the reactants and the corresponding SEM micrographs. The space group is indicated in each case.

Figure 2. Pressure evolution versus time inside the vial to obtain all the composites: (**T**) TiB_2-Al_2O_3, (**Z**) ZrB_2-Al_2O_3, (**H**) HfB_2-Al_2O_3, (**TZ**) $(Ti_{0.5}Zr_{0.5})B_2$-Al_2O_3, (**ZH**) $(Zr_{0.5}Hf_{0.5})B_2$-Al_2O_3 and (**TH**) $(Ti_{0.5}Hf_{0.5})B_2$-Al_2O_3. The maximum pressure indicates the ignition time for all the MSR reactions.

Figure 3. X-ray diffraction patterns corresponding to the TiB_2-Al_2O_3 composite directly after ignition ($\mathbf{T_a}$) compared with the same composite milled for 2 additional hours (**T**).

Figure 4. X-ray diffraction patterns of the obtained composites: (a) **T**, **Z** and **TZ**; (b) **T**, **H** and **TH;** and (c) **Z**, **H** and **ZH** compared with the diboride solid solutions.

Figure 5. (a) SEM micrographs corresponding to the obtained composites: (**T**) TiB_2-Al_2O_3, (**Z**) ZrB_2-Al_2O_3, (**H**) HfB_2-Al_2O_3, (**TZ**) $(Ti_{0.5}Zr_{0.5})B_2$-Al_2O_3, (**TH**) $(Ti_{0.5}Hf_{0.5})B_2$-Al_2O_3 and (**ZH**) $(Zr_{0.5}Hf_{0.5})B_2$-Al_2O_3. (b) SE image and elemental maps of the **TH** composite.

Figure 6. TEM, ED and EDX representative results corresponding to the (**T**) TiB_2-Al_2O_3 and (**TH**) $(Ti_{0.5}Hf_{0.5})B_2$-Al_2O_3 composites.

Table I. Equations, ΔH^o [25] and ignition time values of the reactions to form the six composites: **T** (TiB_2-Al_2O_3); **Z** (ZrB_2-Al_2O_3); **H** (HfB_2-Al_2O_3); **TZ** ($Ti_{0.5}Zr_{0.5}B_2$-Al_2O_3); **TH** ($Ti_{0.5}Hf_{0.5}B_2$-Al_2O_3) and **ZH** ($Zr_{0.5}Hf_{0.5}B_2$-Al_2O_3). Data of formation enthalpies for the ternary diborides are not available in the literature; the averaged values from the formation enthalpies of the binary compounds have been used.

$6HBO_2 + 6Al \rightarrow 6B + 3Al_2O_3 + 3H_2O$ $3TiO_2 + 4Al \rightarrow 3Ti + 2Al_2O_3$ $3Ti + 6B \rightarrow 3TiB_2$ $3TiO_2 + 6HBO_2 + 10Al \rightarrow \mathbf{3TiB_2 + 5Al_2O_3} + 3H_2O$ **(1) T**	ΔH^o =-1132.50 *kJ* ΔH^o = -527.20 *kJ* ΔH^o = -947.70 *kJ* ΔH^o =-2607.40 *kJ* **t_i = 16.5 min.**
$6HBO_2 + 6Al \rightarrow 6B + 3Al_2O_3 + 3H_2O$ $3ZrO_2 + 4Al \rightarrow 3Zr + 2Al_2O_3$ $3Zr + 6B \rightarrow 3ZrB_2$ $3ZrO_2 + 6HBO_2 + 10Al \rightarrow \mathbf{3ZrB_2 + 5Al_2O_3} + 3H_2O$ **(2) Z**	ΔH^o =-1132.50 *kJ* ΔH^o = -49.60 *kJ* ΔH^o = -971.40 *kJ* ΔH^o =-2153.50 *kJ* **t_i = 22.3 min.**
$6HBO_2 + 6Al \rightarrow 6B + 3Al_2O_3 + 3H_2O$ $3HfO_2 + 4Al \rightarrow 3Hf + 2Al_2O_3$ $3Hf + 6B \rightarrow 3HfB_2$ $3HfO_2 + 6HBO_2 + 10Al \rightarrow \mathbf{3HfB_2 + 5Al_2O_3} + 3H_2O$ **(3) H**	ΔH^o =-1132.50 *kJ* ΔH^o = 1.10 *kJ* ΔH^o = -986.70 *kJ* ΔH^o =-2118.10 *kJ* **t_i = 19.9 min.**
$6HBO_2 + 6Al \rightarrow 6B + 3Al_2O_3 + 3H_2O$ $3/2TiO_2 + 2Al \rightarrow 3/2Ti + Al_2O_3$ $3/2ZrO_2 + 2Al \rightarrow 3/2Zr + Al_2O_3$ $3/2Ti + 3/2Zr + 6B \rightarrow 3(Ti_{0.5}Zr_{0.5})B_2$ $3/2TiO_2 + 3/2ZrO_2 + 6HBO_2 + 10Al \rightarrow \mathbf{3(Ti_{0.5}Zr_{0.5})B_2 + 5Al_2O_3} + 3H_2O$ **(4) TZ**	ΔH^o =-1132.50 *kJ* ΔH^o = -263.60 *kJ* ΔH^o = -24.80 *kJ* ΔH^o = -959.50 *kJ* ΔH^o =-2380.40 *kJ* **t_i = 20.6 min.**
$6HBO_2 + 6Al \rightarrow 6B + 3Al_2O_3 + 3H_2O$ $3/2TiO_2 + 2Al \rightarrow 3/2Ti + Al_2O_3$ $3/2HfO_2 + 2Al3 \rightarrow 3/2Hf + Al_2O_3$ $3/2Ti + 3/2Hf + 6B \rightarrow 3(Ti_{0.5}Hf_{0.5})B_2$ $3/2TiO_2 + 3/2HfO_2 + 6HBO_2 + 10Al \rightarrow \mathbf{3(Ti_{0.5}Hf_{0.5})B_2 + 5Al_2O_3} + 3H_2O$ **(5) TH**	ΔH^o =-1132.50 *kJ* ΔH^o = -263.60 *kJ* ΔH^o = 0.55 *kJ* ΔH^o = -967.20 *kJ* ΔH^o =-2362.75 *kJ* **t_i = 17.6 min.**
$6HBO_2 + 6Al \rightarrow 6B + 3Al_2O_3 + 3H_2O$ $3/2ZrO_2 + 2Al \rightarrow 3/2Zr + Al_2O_3$ $3/2HfO_2 + 2Al3 \rightarrow 3/2Hf + Al_2O_3$ $3/2Zr + 3/2Hf + 6B \rightarrow 3(Zr_{0.5}Hf_{0.5})B_2$ $3/2ZrO_2 + 3/2HfO + 6HBO_2 + 10Al \rightarrow \mathbf{3(Zr_{0.5}Hf_{0.5})B_2 + 5Al_2O_3} + 3H_2O$ **(6) ZH**	ΔH^o =-1132.50 *kJ* ΔH^o = -24.80 *kJ* ΔH^o = 0.55 *kJ* ΔH^o = -979.10 *kJ* ΔH^o =-2135.85 *kJ* **t_i = 23.8 min.**

Table II. Structural parameters of the used reactants to carry out the self-propagating reactions by mechanical milling.

	Symmetry	**Cell parameters (nm) (º)**	**Space group**	**Main particle size (nm)**
Al	Cubic	a=0.405	F_{m3m} (25)	10000
HBO_2	Monoclinic	a=0.712; α=90 b=0.884 β=93.26 c=0.677; γ=90	$P_{21/a}$ (14)	200
TiO_2	Tetragonal (anatase)	a=0.378 c=0.950	$I_{41/amd}$ (41)	150
ZrO_2	Monoclinic	a=0.532; α=90 b=0.521; β=99.22 c=0.515; γ=90	$P_{21/a}$ (14)	100
HfO_2	Monoclinic	a=0.528; α=90 b=0.518; β=99.25 c=0.512; γ=90	$P_{21/a}$ (14)	100

Table III. Phase quantification (%wt,), diboride lattice parameters and goodness of fitness obtained by Rietveld analysis in the studied nanocomposites.

Nano-composite	**Al_2O_3**	**XB_2**		**XO_2**	χ^2
	%wt.	**%wt.**	***a*, *c*** (Å)	**%wt.**	
T	73.9	26.1	3.032, 3.232		1.28
Z	51.3	36.4	3.169, 3.529	12.2	4.07
H	46.3	41.4	3.143, 3.476	12.3	4.07
TZ	60.2	34.5	3.091, 3.375	5.3	1.51
TH	48.0	42.2	3.080, 3.347	9.8	1.90
ZH	46.1	49.6	3.158, 3.504	4.3	2.28

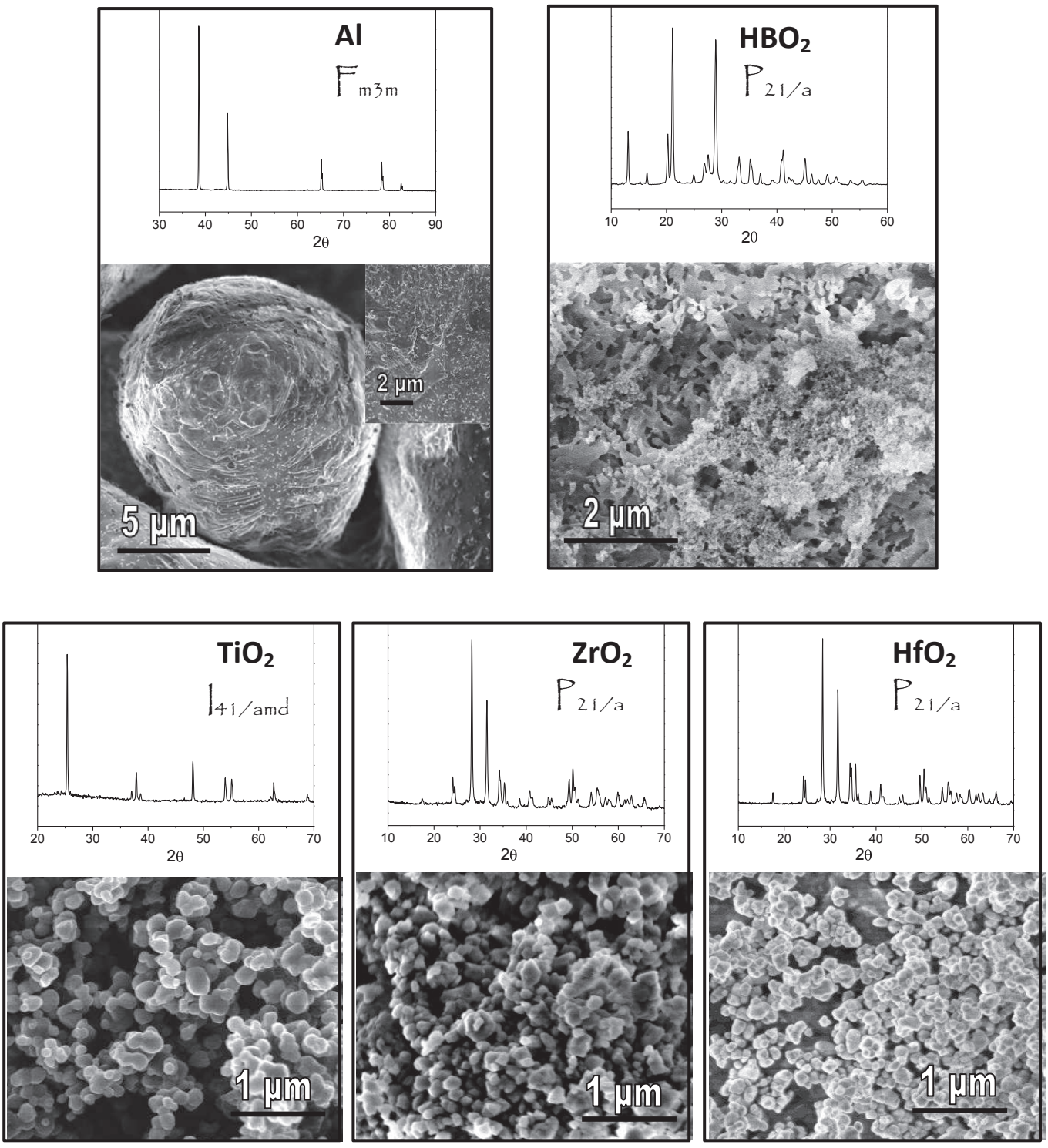
Al
Fm3m
30 40 50 60 70 80 90
2θ
2 μm
5 μm
HBO2
P21/a
10 20 30 40 50 60
2θ
2 μm
TiO2
I41/amd
20 30 40 50 60 70
2θ
1 μm
ZrO2
P21/a
10 20 30 40 50 60 70
2θ
1 μm
HfO2
P21/a
10 20 30 40 50 60 70
2θ
1 μm

Figure 1

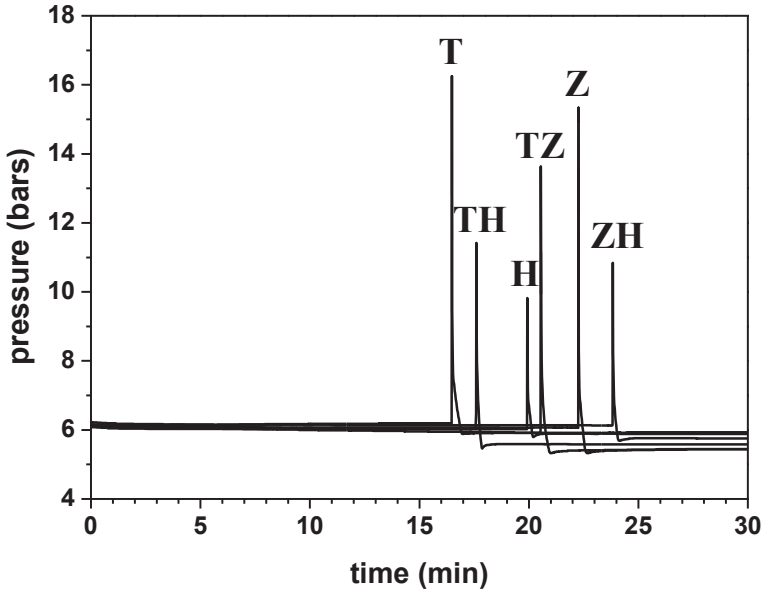
T
Z
TZ
TH
ZH
H
pressure (bars)
time (min)
18
16
14
12
10
8
6
4
0
5
10
15
20
25
30

Figure 2

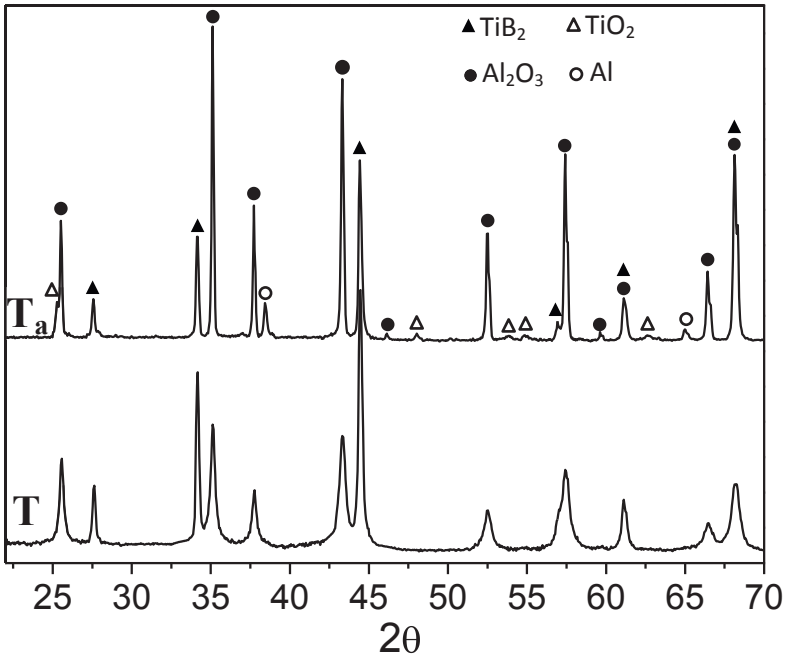

Figure 3

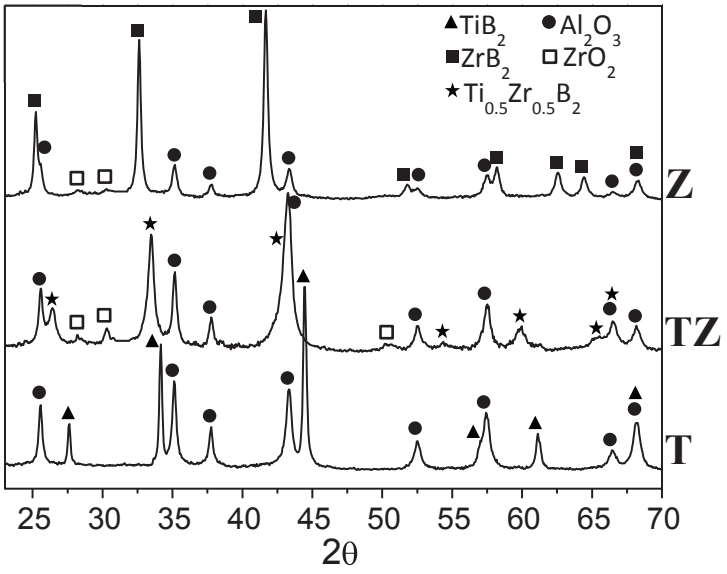
TiB2
Al2O3
ZrB2
ZrO2
Ti0.5Zr0.5B2
Z
TZ
T
25 30 35 40 45 50 55 60 65 70
2θ

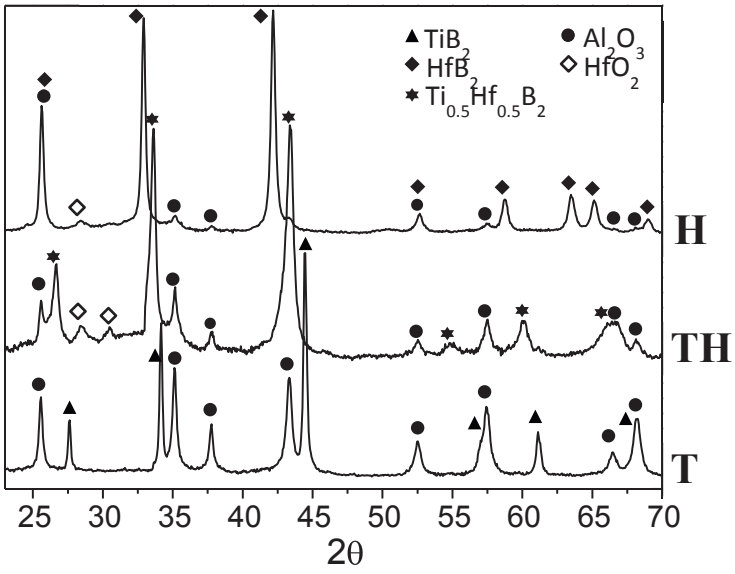
TiB2
Al2O3
HfB2
HfO2
Ti0.5Hf0.5B2
H
TH
T
25 30 35 40 45 50 55 60 65 70
2θ

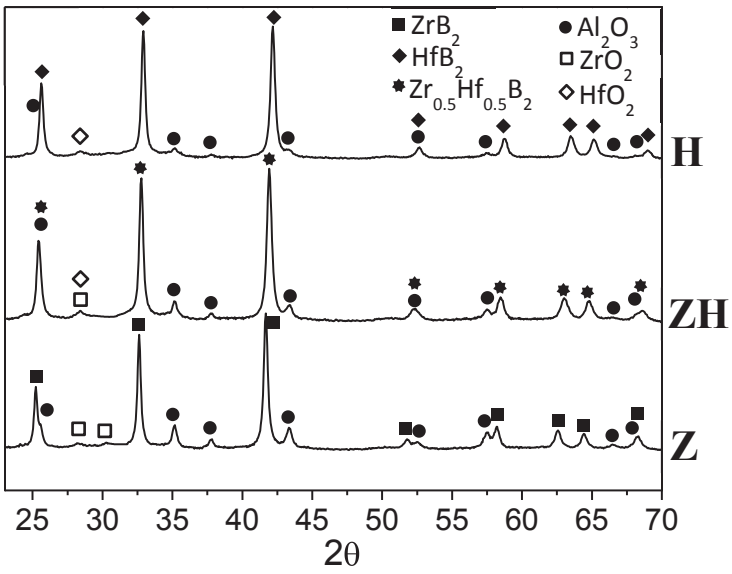
ZrB2
Al2O3
HfB2
ZrO2
Zr0.5Hf0.5B2
HfO2
H
ZH
Z
25 30 35 40 45 50 55 60 65 70
2θ

Figure 4

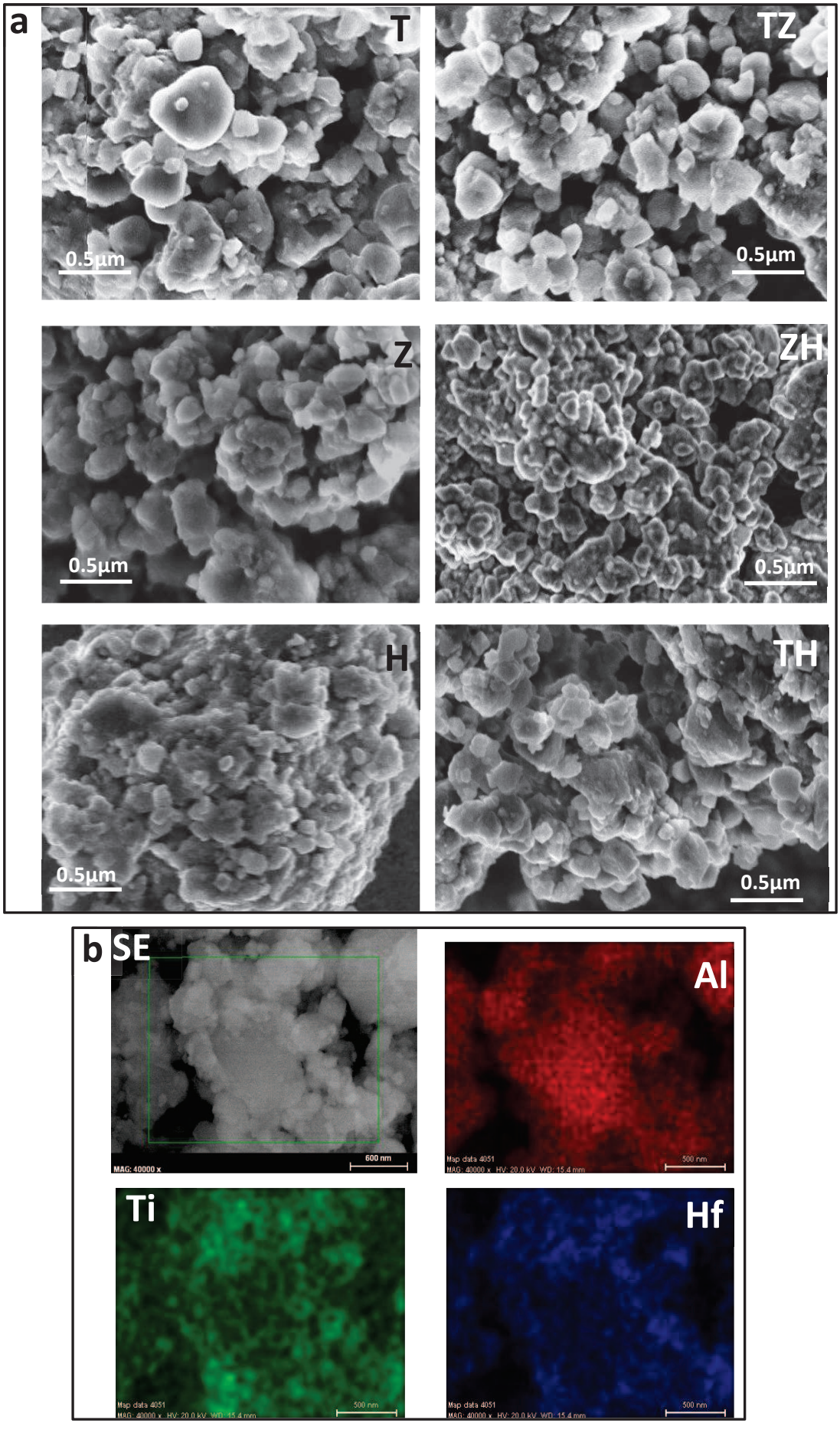
a
T
0.5μm
TZ
0.5μm
Z
0.5μm
ZH
0.5μm
H
0.5μm
TH
0.5μm
b
SE
MAG: 40000 x
600 nm
Al
Map data 4051
MAG: 40000 x HV: 20.0 kV WD: 15.4 mm
500 nm
Ti
Map data 4051
MAG: 40000 x HV: 20.0 kV WD: 15.4 mm
500 nm
Hf
Map data 4051
MAG: 40000 x HV: 20.0 kV WD: 15.4 mm
500 nm

Figure 5

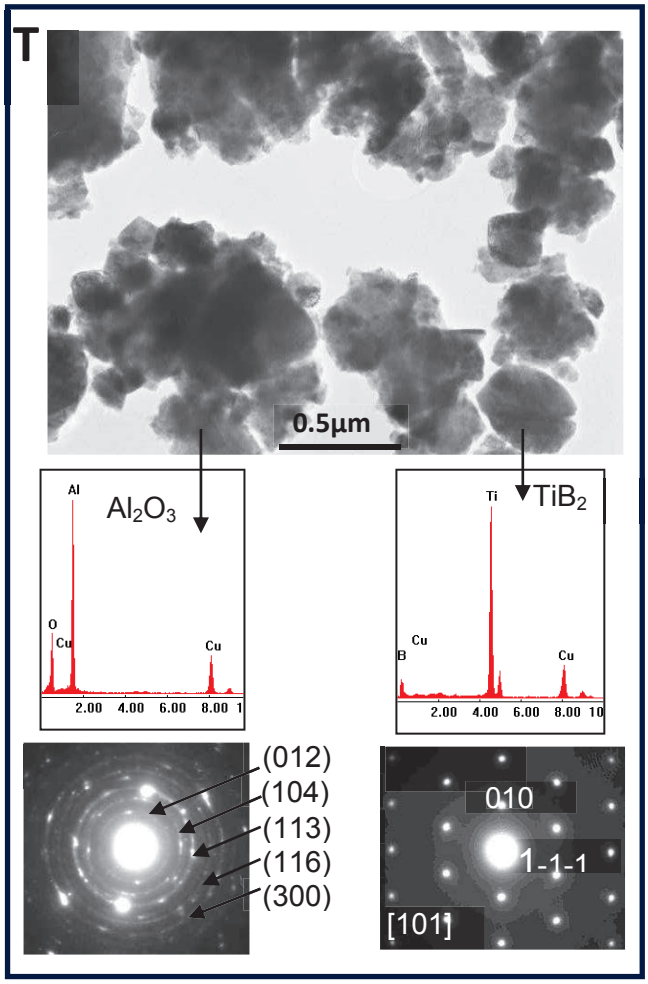
T
0.5µm
Al
Al_2O_3
O
Cu
Cu
2.00 4.00 6.00 8.00 1
Ti
TiB_2
Cu
B
Cu
2.00 4.00 6.00 8.00 10
(012)
(104)
(113)
(116)
(300)
010
1-1-1
[101]

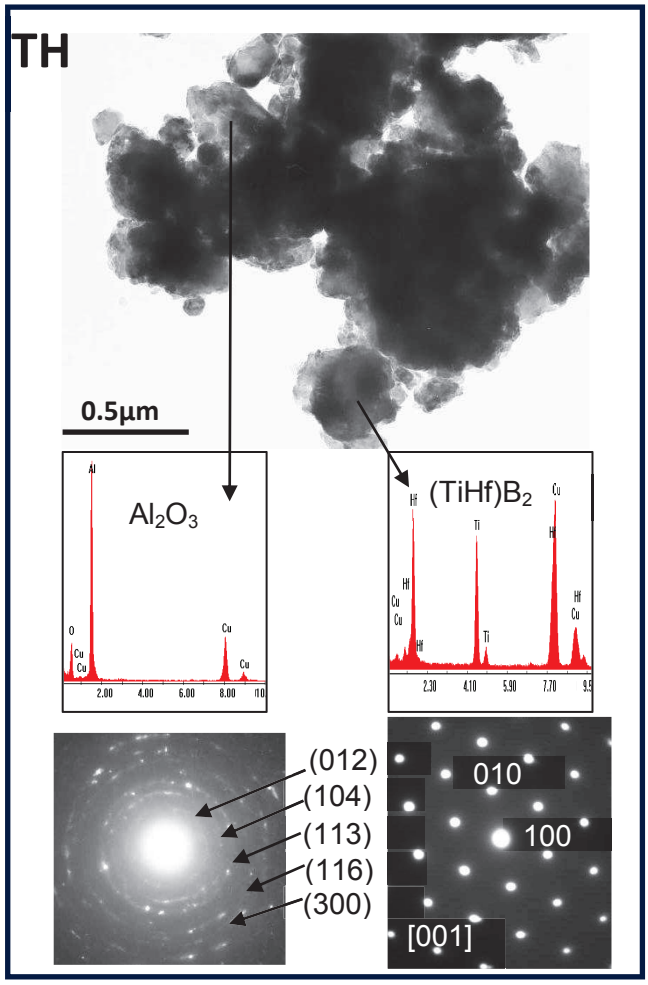
TH
0.5µm
Al
Al_2O_3
O
Cu
Cu
Cu
2.00 4.00 6.00 8.00 10
Hf
$(TiHf)B_2$
Ti
Cu
Hf
Cu
Hf
Ti
Hf
Cu
2.30 4.10 5.90 7.70 9.5
(012)
(104)
(113)
(116)
(300)
010
100
[001]

Figure 6